1521-0103/363/2/164–175$25.00
THE JOURNAL OF PHARMACOLOGY AND EXPERIMENTAL THERAPEUTICS

https://doi.org/10.1124/jpet.117.242164
J Pharmacol Exp Ther 363:164–175, November 2017

Depletion of Progranulin Reduces GluN2B-Containing NMDA Receptor Density, Tau Phosphorylation, and Dendritic Arborization in Mouse Primary Cortical Neurons[S]

Francesca Longhena, Michela Zaltieri, Jessica Grigoletto, Gaia Faustini, Luca La Via, Roberta Ghidoni, Luisa Benussi, Cristina Missale, PierFranco Spano, and Arianna Bellucci

Department of Molecular and Translational Medicine, University of Brescia, Brescia, Italy (F.L, M.Z., J.G., G.F., L.L.V., C.M., P.S., A.B.) and Molecular Markers Laboratory, IRCCS Instituto Centro San Giovanni di Dio Fatebenefratelli, Brescia, Italy (R.G., L.B.)

ABSTRACT

Loss-of-function mutations in the progranulin (PGRN) gene are a common cause of familial frontotemporal lobar degeneration (FTLD). This age-related neurodegenerative disorder, characterized by brain atrophy in the frontal and temporal lobes and such typical symptoms as cognitive and memory impairment, profound behavioral abnormalities, and personality changes is thought to be related to connectome dysfunctions. Recently, PGRN reduction has been found to induce a behavioral phenotype reminiscent of FTLD symptoms in mice by affecting neuron spine density and morphology, suggesting that the protein can influence neuronal structural plasticity. Here, we evaluated whether a partial haploinsufficiency-like PGRN depletion, achieved by using RNA interference in primary mouse cortical neurons, could modulate GluN2B-containing *N*-methyl-D-aspartate (NMDA) receptors and tau phosphorylation, which are crucially involved in the regulation of the structural plasticity of these cells. In addition, we studied the effect of PGRN decrease on neuronal cell arborization both in the presence and absence of GluN2B-containing NMDA receptor stimulation. We found that PGRN decline diminished GluN2B-containing NMDA receptor levels and density as well as NMDA-dependent tau phosphorylation. These alterations were accompanied by a marked drop in neuronal arborization that was prevented by an acute GluN2B-containing NMDA receptor stimulation. Our findings support that PGRN decrease, resulting from pathogenic mutations, might compromise the trophism of cortical neurons by affecting GluN2B-contaning NMDA receptors. These mechanisms might be implicated in the pathogenesis of FTLD.

Introduction

Progranulin (PGRN), also known as granulin (GRN)-epithelin precursor, is a secreted pleiotropic growth factor controlling the maintenance and regulation of the homeostatic dynamics of normal tissue development, proliferation, regeneration, immunity, and inflammation (Jian et al., 2013; Petkau and Leavitt, 2014). Its role has been widely studied in the field of infectious diseases, wound healing, tumorigenesis, and most recently, neurodegenerative diseases. Indeed, GRN nonsense mutations, producing aberrant mRNA transcripts undergoing non-sense–mediated decay, have been found to be responsible for the onset of familial forms of frontotemporal lobar degeneration (FTLD) (Baker et al., 2006; Cruts et al., 2006; Gijselinck et al., 2008; Skoglund et al., 2011). All the pathogenic GRN mutations identified thus far cause the disease through a uniform mechanism, i.e., loss of functional progranulin or haploinsufficiency with FTLD resulting from progranulin depletion rather than from the accumulation of the mutant protein (Ghidoni et al., 2008, 2012) (Finch et al., 2009; Sleegers et al., 2009). FTLD is a neurodegenerative disorder characterized by prominent atrophy of the frontal and temporal lobes of the brain and occurring in mid-life and later. The typical symptoms encompass profound behavioral abnormalities, personality changes, progressive aphasia, as well as other types of cognitive and memory impairment (McKhann et al., 2001).

In FTLD patients carrying a GRN mutation, the main pathologic signature on magnetic resonance imaging is the involvement of the fronto-temporo-parietal circuits, with prominent parietal and asymmetric atrophy (Whitwell et al., 2007; Rohrer et al., 2010; Bozzali et al., 2013), impaired connectivity in long-distance intrahemispheric tracts (Rohrer et al., 2013), salience network disruption (Borroni et al., 2012), and impaired brain oscillatory activity (Moretti et al., 2016).

Cortical atrophy and white matter tract abnormalities in frontal-parietal circuits can be detected at least a decade before the estimated onset of symptoms in asymptomatic mutation carriers (Pievani et al., 2014; Rohrer et al., 2015), suggesting that connectome dysfunctions could be crucial for disease manifestation.

In the brain, PGRN is expressed in both microglial cells and neurons but not in astrocytes. Although GRN expression in neurons increases with cell maturation, its expression in microglia varies in relation to the activation state of the cells and can be enhanced in response to excitotoxic injury (Petkau et al.,

This work was supported by the Fondazione Cariplo Project 2009-2633, and by the Italian Ministry of Education, Universities, and Research (Ex 60%).
doi.org/10.1124/jpet.117.242164.
[S] This article has supplemental material available at jpet.aspetjournals.org.

ABBREVIATIONS: ANOVA, analysis of variance; BSA, bovine serum albumin; DIV, day(s) in vitro; FTLD, frontotemporal lobar degeneration; GRN, granulin; ICC, immunocytochemistry; IHC, immunohistochemistry; KRS, Krebs-Ringer solution; LDH, lactate dehydrogenase; NMDA, *N*-methyl-D-aspartate; P0, newborn; PBS, phosphate-buffered saline; PRGN, progranulin; RNAi, RNA interference; SCR, scramble.

2010). Complete deficiency of PGRN has been found to dysregulate microglial activation, contribute to increased neuron loss with injury, and promote circuit-specific synaptic pruning via complement activation (Lui et al., 2016; Martens et al., 2012). However, more recent studies reported differences in the effect of protein deficiency in multiple inbred mouse strains in relation to neuron spine density and morphology (Petkau et al., 2016), thus suggesting a complex role for PGRN in the regulation of neuronal resilience. Consistently, a biased lack of PGRN in mice can induce behavioral abnormalities that are reminiscent of FTLD symptoms such as age-dependent social and emotional deficits. These alterations occur in the absence of gliosis or increased expression of tumor necrosis factor-α, thus suggesting that FTLD-related deficits can develop in the absence of detectable neuroinflammatory changes, and supporting an important effect of PGRN deficiency on neurons (Filiano et al., 2013). On the other hand, both full length PGRN and GRN-epithelin peptide promote neuronal survival and neurite outgrowth in primary rat cortical and motor neurons (Van Damme et al., 2008; Ryan et al., 2009). PGRN has also been implicated in the regulation of motor neuron development as well as neurite outgrowth and branching (Chitramuthu et al., 2010; Laird et al., 2010), and gene silencing of PGRN in primary hippocampal neurons affects neuronal connectivity (Tapia et al., 2011). In line with this evidence, we demonstrated (Benussi et al., 2016) that the presence of GRN null mutations strongly reduces the number of released exosomes, microvesicles serving as intercellular communication tools that can be released by neurons following synaptic activation (Laulagnier et al., 2017).

Collectively, these studies support the conclusion that PGRN deficiency can affect neuronal structural plasticity.

Of note, this latter process can be finely regulated by the activity of glutamate *N*-methyl-D-aspartate (NMDA) receptors (Carpenter-Hyland and Chandler, 2007; Mony et al., 2009; Wyllie et al., 2013; Stein et al., 2015), those containing the GluN2B subunit in particular (Williams et al., 2003; El Gaamouch et al., 2012). GluN2B-containing NMDA receptors have been found to be implicated in the control of tau phosphorylation in cortical and hippocampal neurons (Laurier-Laurin et al., 2014; Arendt et al., 2015) and NMDA receptors can mediate tau-dependent neuronal degeneration (Tackenberg et al., 2013). Therefore, the resilience of cortical and hippocampal neurons, which are vulnerable in FTLD, may be particularly sensitive to subtle homeostatic changes in NMDA receptor function and tau post-translational modifications.

On this basis, we aimed at studying whether and how PGRN reduction could modulate the structural plasticity of primary cortical neurons by affecting the expression of NMDA receptors and tau phosphorylation. We found that PGRN gene silencing decreased GluN2B-containing NMDA receptor density and activity as well as NMDA-dependent tau phosphorylation without affecting cell viability. These events were accompanied by the onset of a marked reduction in dendritic arborization of cortical neurons that could be prevented by an acute stimulation of GluN2B-containing NMDA receptors.

Materials and Methods

Animals. C57BL/6J mice were used to prepare primary neuronal cell cultures and to characterize PGRN expression in the adult brain. Animals were bred and housed in the Animal House facility of the Department of Molecular and Translational Medicine of the University of Brescia with food and water and maintained on a 12-hour light/dark cycle at a room temperature 23°C. All experiments and surgical procedures conformed to the National Research Guide for the Care and Use of Laboratory Animals and were approved by the Animal Research Committees of the University of Brescia (protocol permit nos. 03/12 and 04/12). All efforts were made to minimize animal suffering and to reduce the number of animals used.

Primary Cortical and Hippocampal Neuronal Cultures. Primary neuronal cultures from cortical and hippocampal tissues were dissected from C57BL/6J newborn pups at day 0. Briefly, after mechanical dissociation the single cells were resuspended in Neurobasal-A medium (Gibco/Thermo Fisher Scientific, Milan, Italy), containing 100 μg/ml penicillin, 100 μg/ml streptomycin (Sigma-Aldrich, Milan, Italy), 0.5 mM glutamine (EuroClone, Milan, Italy), and 1% B27 supplement (Gibco). Cells were then centrifuged, and cell count and viability assays were performed using the Trypan blue exclusion test. Cells were seeded onto poly-D-lysine-coated glass coverslides in 24-well plates (14 μg/ml) for immunocytochemistry (70,000 cells/well), or onto poly-D-lysine-coated Petri dishes (10 μg/ml) for biochemical analyses (800,000 cells/dish). Cells were maintained at 37°C under a humidified atmosphere of 5% CO_2 and 95% O_2 for at least 10 days in vitro (DIV) to allow their maturation prior to their use. Characterization experiments on cell cultures showed that they contained 95% neuronal cells and 5% astrocytes (results not shown).

RNA Interference. Cortical neurons were subjected to RNA interference (RNAi) at DIV 10 with four different siRNA sequences for PGRN gene silencing (Dharmacon, Chicago, IL). A nonsilencing RNA sequence, scramble (SCR), was used as negative control. The optimal targeting and SCR RNA concentrations for gene silencing were estimated to be 25 nM.

All the sequences were diluted in Opti-MEM (Gibco) and then transfected into cells using INTERFERin (Polyplus-Transfection, Illkirch, France) according to the manufacturer' s instructions.

Lactate Dehydrogenase Activity–Based Cytotoxicity Assay. Cell culture media from either control primary neuronal cultures or cultures treated with siRNA or SCR were centrifuged at 250*g* for 4 minutes to remove the cells debris. Lactate dehydrogenase (LDH) activity measurements were performed using a commercially available assay (Sigma-Aldrich) according to the manufacturer's instructions. The LDH activity was measured at 490 and 600 nm with a spectrophotometer.

Measurement of Intracellular Calcium Concentrations. Regulation of cytosolic free Ca^{2+} concentration by NMDA in primary cortical neuronal cells was investigated by microfluorimetry in single cells according to Navarria et al. (2015). The cells were plated onto 50-ng/ml poly-L-lysine–coated glass coverslips at a density of 0.5×10^3 cells/cm^2 and cultured as described above. At DIV 10, cells were loaded with the Ca^{2+}-sensitive fluorescent dye Fura-2 AM (Sigma-Aldrich). Incubation was carried out for 60 minutes at 37°C in Krebs-Ringer solution (KRS) (125 mM NaCl, 5 mM KCl, 1.2 mM KH_2PO_4, 2 mM $CaCl_2$, 25 mM HEPES–NaOH, 6 mM glucose, pH 7.4) containing 1.3 mg/ml bovine serum albumin (BSA) and 4 mM Fura-2 AM. They were then mounted in a 22-mm holder creating a chamber with the coverslips on the bottom. Fura-2 emission was monitored by using an inverted fluorescence microscope (Nikon Diaphot) associated with an intensified charge-coupled device camera (MIRA-100 TE; Applied Imaging, Gateshead, UK), which recorded the 510-nm fluorescence emission in neurons excited through narrow band-pass filters (340 and 380 nm). The background was subtracted and the amount of free Ca^{2+} within the cell bodies was calculated from the ratio of 340/380 nm obtained every 3 − 4 seconds. Calibration was made according to external standards of Ca^{2+} and Fura-2. Fluorescent image acquisition and analysis were performed using the MIRAcal (Multiple Image Ratioing and Analysis with Calibration System; Applied Imaging, Gateshead, UK). Cells were exposed to 500 μM NMDA and 100 μM glycine for 200 seconds in the chamber containing Mg^{2+}-free KRS. To check whether Ca^{2+} release was dependent

on GluN2B-containing NMDA receptors, cells were exposed to 1 μM ifenprodil, which was added 30 seconds before glutamate and glycine stimulation and maintained for the entire experiment. Cells were then washed with Ca^{2+}-free solution and returned to the KRS. To check whether analyzed cells were sensitive to depolarizing stimuli, at the end of each experiment, 100 mM KCl stimulation was performed. Plateau values of $[Ca^{2+}]$ increase were calculated from the mean of four determinations taken at 20, 40, 60, 80, and 120 seconds after application of stimulating agents.

Cell Culture Treatments. To evaluate the effect of NMDA receptor stimulation on neuronal arborization and tau phosphorylation in siRNA-exposed neurons, at 24 hours from gene silencing the cells were exposed to 500 μM NMDA and 100 μM glycine in Mg^{2+}-free KRS for 10 minutes. Pretreatment with the GluN2B antagonist ifenprodil was performed in the same conditions with the addition of 10 μM ifenprodil to Mg^{2+}-free KRS 20 minutes prior to NMDA + glycine. Cells were then incubated again with their original cell culture media. A fraction of siRNA-exposed cells were subjected to media changes without the addition of NMDA and glycine as a control.

Immunocytochemistry. For immunocytochemistry (ICC) cells were fixed by incubation for 15 minutes in 3% paraformaldehyde/3% sucrose made up in phosphate-buffered saline (PBS) 1 M, pH 7.4, and then stored in PBS containing 0.05% sodium azide. Slides were incubated for 10 minutes at 25°C in a permeabilization solution composed by 20% methanol in PBS containing 0.1% Triton X-100, then 30 minutes in blocking solution composed by 2% (v/v) normal goat serum (Sigma-Aldrich) plus 3% (w/v) BSA (Sigma-Aldrich) in PBS containing 0.1% Triton X-100, and then overnight at 4°C with primary antibody at the optimal working dilution made up in blocking solution. On the following day, cells were incubated for 1 hour at 25°C with the fluorescent secondary antibody diluted in PBS containing 0.1% Triton X-100 with 0.1% BSA. For double-labeling, at the end of this incubation cells underwent another cycle of staining. Cell nuclei were counterstained with Hoechst 2495 (Sigma-Aldrich). Coverslips were then mounted on glass slides with Vectashield mounting medium (Vector Laboratories, Burlingame, CA).

Immunohistochemistry. For immunohistochemistry (IHC), mice were anesthetized with chloral hydrate (400 mg/kg, i.p.) and were perfused transcardially with 4% ice-cold paraformaldehyde in 0.1 M phosphate buffer, pH 7.2. For newborn (P0) pups, mice were decapitated and the whole head was fixed in 4% ice-cold paraformaldehyde overnight. At 4 hours postfixation, brains were put in 18% sucrose, and the day after, 30-μm coronal sections were cut with a cryostat (Leica Biosystems, Nußloch, Germany).

Free-floating sections were washed with PBS containing 0.3% Triton X-100 and incubated for 30 minutes at 25°C in a permeabilization solution composed by 20% methanol in PBS containing 0.3% Triton X-100, then 1 hour in blocking solution composed by 2% (v/v) normal goat serum (Sigma-Aldrich) plus 3% (w/v) bovine serum albumin (BSA; Sigma-Aldrich) in PBS containing 0.3% Triton X-100, and then overnight at 4°C with primary antibody at the optimal working dilution made up in blocking solution. On the following day, cells were incubated for 1 hour at 25°C with the fluorescent secondary antibody diluted in PBS containing 0.3% Triton X-100 with 0.1% BSA. For double-labeling, at the end of this incubation, cells underwent another cycle of staining. Cell nuclei were counterstained with Hoechst 2495 (Sigma-Aldrich). Coverslips were then mounted on glass slides with the Vectashield mounting medium (Vector Laboratories).

Antibodies. A list of the primary antibodies used for this study is summarized in Table 1. Secondary antibodies used for IHC and ICC were anti-mouse Cy3-conjugated, anti-rabbit Cy3- or FITC-conjugated (Jackson ImmunoResearch, Baltimore, MD), and anti-sheep ALEXA-488-conjugated (Molecular Probes, Eugene, OR).

Secondary antibodies used for Western blot were anti-mouse, anti-rabbit (Santa Cruz Biotechnology, Santa Cruz, CA) and anti-sheep (Southern Biotech, Birmingham, AL) horseradish peroxidase–conjugated.

Confocal and Fluorescence Microscopy. Fixed cells and mouse brain sections were observed by means of an inverted light/epifluorescence microscope (Olympus IX50; Olympus, Milan, Italy) or by means of a Zeiss confocal laser microscope (Carl Zeiss S.p.A., Milan, Italy), with the laser set on l = 405–488–543 nm and the height of the sections scanning = 1 μm. Images (512 × 512 pixels) were then reconstructed using LSM Image Examiner (Carl Zeiss S.p.A) and Adobe Photoshop 7.0 (Adobe Systems, Mountain View, CA) software.

Sholl Analysis. A Sholl analysis of single neurons in the primary cortical neuronal cell cultures was performed manually on the basis of ImageJ software (NIH, Bethesda, MD). After MAP-2 ICC, randomly chosen neurons were analyzed. The number of intersections of the neurite tree with increasing circular perimeters from the center of the soma was counted every 30 μm by using a calibrated concentric circle mask. The collected data were plotted by using GraphPad Prism 4 and analyzed as described below.

Western Blot. For total protein extraction, either cell pellets or mouse brain tissue was lysed in a buffer containing 50 mM Tris-HCl, pH 7.4, 150 mM NaCl, 0.5% Na deoxycholate, 0.1% Na dodecyl sulfate, 2 mM EDTA, 0.1 mM phenylmethylsulfonyl fluoride, 1 mM *N*-ethylmaleimide, 1 mM Na orthovanadate, 1% Nonidet P-40, mM NaF 1, and protease inhibitor cocktail (Roche Diagnostics, Mannheim, Germany). For membrane protein extraction, cell pellets were homogenized in Nonidet P-40 buffer (NaCl 150 mM, 50 mM HEPES, pH 7.4, 1% Nonidet P-40) and nuclei and cell debris were eliminated by centrifugation of the homogenate at 500*g* for 10 minutes at 4°C. Pellets were discarded and supernatants were then centrifuged at 100,000*g* for 1 hour at 4°C. The resulting pellet was then dissolved in lysis buffer and centrifuged at 100,000*g* at 4°C for 1 hour. This final pellet containing membrane fractions was used for Western blot analysis. Protein concentrations in the samples were measured by using the Bradford assay (Pierce, Rockford, IL). Equal amounts of proteins (30 μg) were run on 4–12% Invitrogen Novex NuPAGE 4–12% Bis-Tris Protein Gels (Fisher Scientific, Waltham, MA) and blotted on a polyvinylidene difluoride Immobilon-P membrane (Millipore, Milan, Italy). Densitometric analysis of bands was performed by means of Gel Pro Analyzer version 6.0. (Media Cybernetics, Bethesda, MD). Band densities were normalized to either glyceraldehyde-3-phosphate dehydrogenase or α-tubulin levels as a control of equal loading of samples. For membrane protein extracts GluN1 and GluN2B, bands were normalized to the membrane protein amyloid precursor protein levels as a control for equal loading.

Analysis of GluN2B, GluN1 and PSD-95 Density. Images were obtained by using a Zeiss LSM510 Laser scanning confocal Microscope (Ziess, Oberkochen, Germany) with a 63× oil-immersion objective. All images within a single experiment were acquired using equivalent settings by an individual who was blind to treatment conditions. Neurons were selected at random from each quadrant of the coverslip by PGRN staining. For each neuron, three dendrites were chosen and their length was measured from phase contrast images. To quantify the ICC data from the three dendrites of each neuron, the neurons were chosen randomly for image acquisition and processed using Image J software (10 cells from each condition from three independent experiments were acquired). For each experiment, the efficiency of PGRN gene silencing was confirmed by the analysis of the ICC signal, and images in each channel were captured using the same exposure time across all fixed cells. Images were acquired as grayscale from individual channels and pseudocolor overlays were prepared using Adobe Photoshop. To quantify GluN1, GluN2B, and PSD-95 density per dendrite length in ICC photomicrographs, we selected regions using Image J software, subjected the digital images to a user-defined intensity threshold to select clusters (the same threshold sets were used for each independent experiment), and measured for cluster intensity, number, and area. All imaging and analysis were blind to gene-silencing and treatment condition. All the measurements were normalized to control-cell values.

Statistical Analysis. Each experiment was replicated at least three times, with each experimental condition produced either in duplicate or triplicate. Differences between 88- and 62-kDa PGRN

TABLE 1
List of the primary antibodies used for Western blot, ICC, and IHC

Antibody	Specificity	Source	Dilution			Host
			Western blot	ICC	IHC	
PGRN	AA 18-589	R&D System	1:500	1:400	1:500	Sheep
APP	N-terminal	Millipore	1:500	—	—	Mouse
CD11b	—	AbD Serotec	—	—	1:1000	Rat
GAD-67	—	Millipore	—	1:1000	—	Mouse
GAPDH		Millipore	1:5000	—		Mouse
GFAP	—	DAKO	—	—	1:500	Rabbit
MAP-2		Millipore	—	1:300	—	Rabbit
GluN1	C-terminal	Santa Cruz Biotechnology	1:1500	—	—	Rabbit
GluN2B	C-terminal	Santa Cruz Biotechnology	1:1500	—	—	Rabbit
PHF1	$Tau^{pS396/pS404}$	P. Davies	1:1000	—	—	
PSD-95		Cell Signaling Technology	—	1:1000	—	Mouse
p-TAU(Ser262)	Tau^{pS262}	Santa Cruz Biotechnology	1:1000	—	—	Rabbit
Tau 46	C-terminal	Cell Signaling Technology	1:1000	—	—	Mouse
α-Tubulin		Sigma-Aldrich	1:5000	—	—	Mouse

APP, amyloid precursor protein; GADPH, glyceraldehyde 3-phosphate dehydrogenase; GFAP, glial fibrillary acidic protein.

levels assayed by Western blot in cortical and hippocampal samples from control mice were analyzed by two-way analysis of variance (ANOVA) + Bonferroni's multiple comparison test. Differences in 62-kDa PGRN, GluN1, and GluN2B levels between cortical and hippocampal neurons were analyzed by Student's *t* test. The effect of PGRN gene silencing on PGRN levels and LDH release was analyzed by one-way ANOVA followed by Newman-Keuls postcomparison test. The same analysis was used to evaluate differences in GluN1 and GluN2B levels, intracellular Ca^{2+} load, as well as GluN1, GluN2B, and PSD-95 distribution in control, SCR-treated, and siRNA-exposed cells. Two-way ANOVA + Bonferroni's postcomparison test was used to analyze the data from Sholl analysis.

Results

Age-Related Differences in the Expression of the Mature 62-kDa and Glycosylated 88-kDa Form of PGRN in Cortical and Hippocampal Extracts of C57BL/6J Mice

Since the aim of this work was to estimate the effect of PGRN reduction in primary neurons, we first probed the expression of PGRN in the cortex and hippocampus of C57BL/6J mice during aging (Fig. 1, A–C). By Western blot analysis we found that newborn mice only express the mature nonglycosylated form of the 62-kDa protein. The expression of this form of the protein was significantly higher in cortical extract compared with hippocampal extracts (Fig. 1, A and C). However, the expression of nonglycosylated PGRN was significantly reduced both in the hippocampus and cortex of 1-, 8-, and 12-month-old mice compared with newborn mice (Fig. 1, A and C). In parallel, the levels of the glycosylated 88-kDa PGRN form, that was low at P0, strongly increased in the cortical and hippocampal extracts from C57BL6J mice along with aging (Fig. 1, A and B). Of note, the levels of 88-kDa glycosylated PGRN in the hippocampal extracts from 12-month-old mice were found to be significantly higher than those observed in 1- and 8-month-old mice (Fig. 1, A and B). Conversely, the levels of 88-kDa PGRN in the cortical extracts of 1-, 8-, and 12-month-old mice were comparable (Fig. 1, A and B).

Characterization of Primary Cortical and Hippocampal Neuronal Cell Cultures

To definitively choose whether to work on cortical or hippocampal neurons we probed PGRN levels in the cell cultures prepared from newborn P0 mice by Western blot. In line with the above observations we found that at 10 DIV these cells only expressed the 62-kDa PGRN form and its levels were significantly higher in cortical neurons compared with hippocampal neurons (Fig. 2A). These findings indicated that cortical neurons may constitute a more representative model to study the effects of PGRN gene silencing in vitro.

Since one of our aims was to probe the effect of PGRN gene silencing on the GluN2B-containing NMDA receptor, we also studied the levels of GluN1 and GluN2B in primary cortical and hippocampal neuronal protein extracts at DIV 10. By Western blot, we found that the expression of GluN1 and GluN2B was significantly higher in cortical neurons compared with hippocampal neurons (Fig. 2B). These changes were not the result of differences in cell maturation, as confirmed by the analysis of neuronal morphology in phase contrast images (Fig. 2C) and by the fact that both cortical and hippocampal neurons showed a good degree of expression of mature neuronal markers such as NeuN (Fig. 2D), MAP-2 (Fig. 2E), and GAD-67 (Fig. 2F).

Experimental Design and Evaluation of PGRN Gene Silencing and Cell Viability

In this study we aimed at evaluating whether PGRN reduction could modulate neuronal structural plasticity through the modulation of GluN2B-containing NMDA receptor and tau phosphorylation. For this reason we used primary cortical neurons cultured for 10 DIV prepared from newborn P0 mice (Fig. 3A). Cells were subjected to silencing RNA (siRNA)–based RNA interference at DIV 10. Four different siRNA sequences (Fig. 3B) were tested. Efficacy of PGRN gene silencing and NMDA and tau phosphorylation were evaluated at 72 hours from RNAi, cell viability was probed at 96 hours from RNAi, whereas neuronal morphology

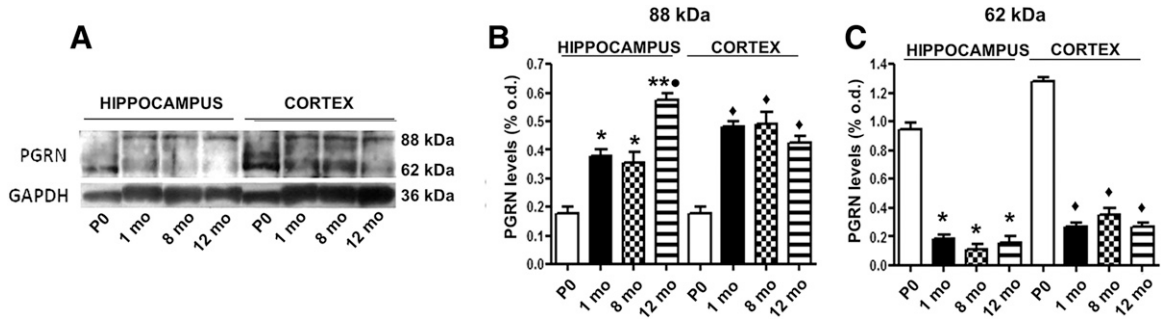

Fig. 1. Levels and distribution of PGRN in the cortex and hippocampus of C57BL/6J mice during aging. (A) Representative Western blot images showing the levels of 62- and 88-kDa PGRN in the hippocampus and cortex of newborn (P0), 1-month-, 8-month-, and 12-month-old mice. Glyceraldehyde-3-phosphate dehydrogenase (GAPDH) bands are shown as a control of sample loading. (B) The histogram shows the mean + S.E.M. optical density (o.d.) of the 88-kDa PGRN-immunopositive bands when normalized to GAPDH bands' o.d. Please note the statistically significant increase of 88-kDa hippocampal and cortical PGRN during mouse aging. $^{*}P < 0.05$ vs. P0, $^{**}P < 0.01$ vs. P0, $\bullet P < 0.05$ vs. 1- and 8-month-old, $\blacklozenge P < 0.001$ vs. P0, two-way ANOVA plus Bonferroni's postcomparison test (N = 4 triplicates for each of the experimental conditions analyzed). (C) Histogram showing the relative o.d. (mean + S.E.M.) of 62-kDa PGRN-immunopositive bands when normalized to o.d of GAPDH bands. A statistically significant decrease in the protein in cortical and hippocampal neurons during mouse aging was evident. $^{*}P < 0.001$ vs. P0; $\blacklozenge P < 0.001$ vs. P0, two-way ANOVA plus Bonferroni's postcomparison tests (N = 4 triplicates for each of the experimental conditions analyzed).

and GluN2B and PGRN expression were analyzed at 120 hours from gene silencing. A schematic representation of our experimental design is showed in Fig. 3A.

By Western blot we found that siRNA sequence 4 was able to induce an efficient 60% reduction in PGRN levels that was evident at 72 hours from RNAi (Fig. 3C), without affecting cell

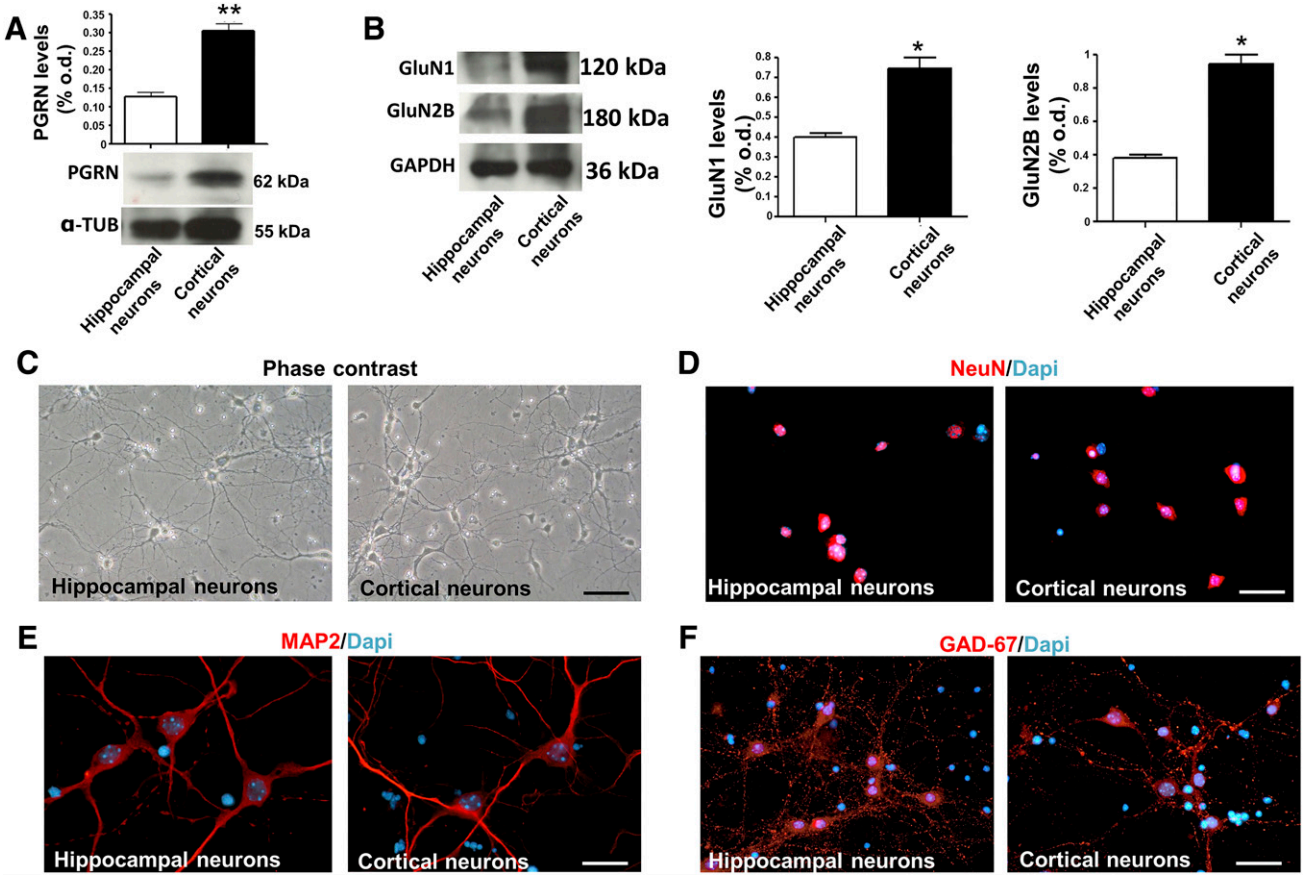

Fig. 2. PGRN- and GluN2B-containing NMDA receptor levels and maturation of primary cortical and hippocampal neuronal cells at 10 DIV. (A) Histogram showing the levels of 62-kDa PGRN (mean +S.E.M.) in primary mouse cortical and hippocampal neurons. Representative immunoblotting bands are shown below the bars. Please note that cortical neurons express higher levels of the protein; $^{**}P < 0.01$ Student's t test (N = 5 triplicates for each group). (B) GluN1 and GluN2B levels in primary mouse cortical and hippocampal neuronal cell cultures. Representative immunoblottings are shown on the left. The histograms show that GluN1 and GluN2B levels (mean + S.E.M.) were significantly higher in cortical neurons than in hippocampal neurons; $^{*}P < 0.001$ Student's t test (N = 4 triplicates for each experimental condition analyzed). (C) Phase contrast images showing the morphology of cortical and hippocampal neuronal cells at 10 DIV. Scale bar, 280 μm. (D) NeuN ICC shows the presence of mature NeuN-positive neurons in both primary cortical and hippocampal neuronal cell cultures. Scale bar, 120 μm. (E) MAP-2 immunopositivity in cortical and hippocampal neurons. Scale bar, 50 μm. (F) GAD-67 ICC shows the presence of mature GABAergic neurons. Scale bar, 100 μm.

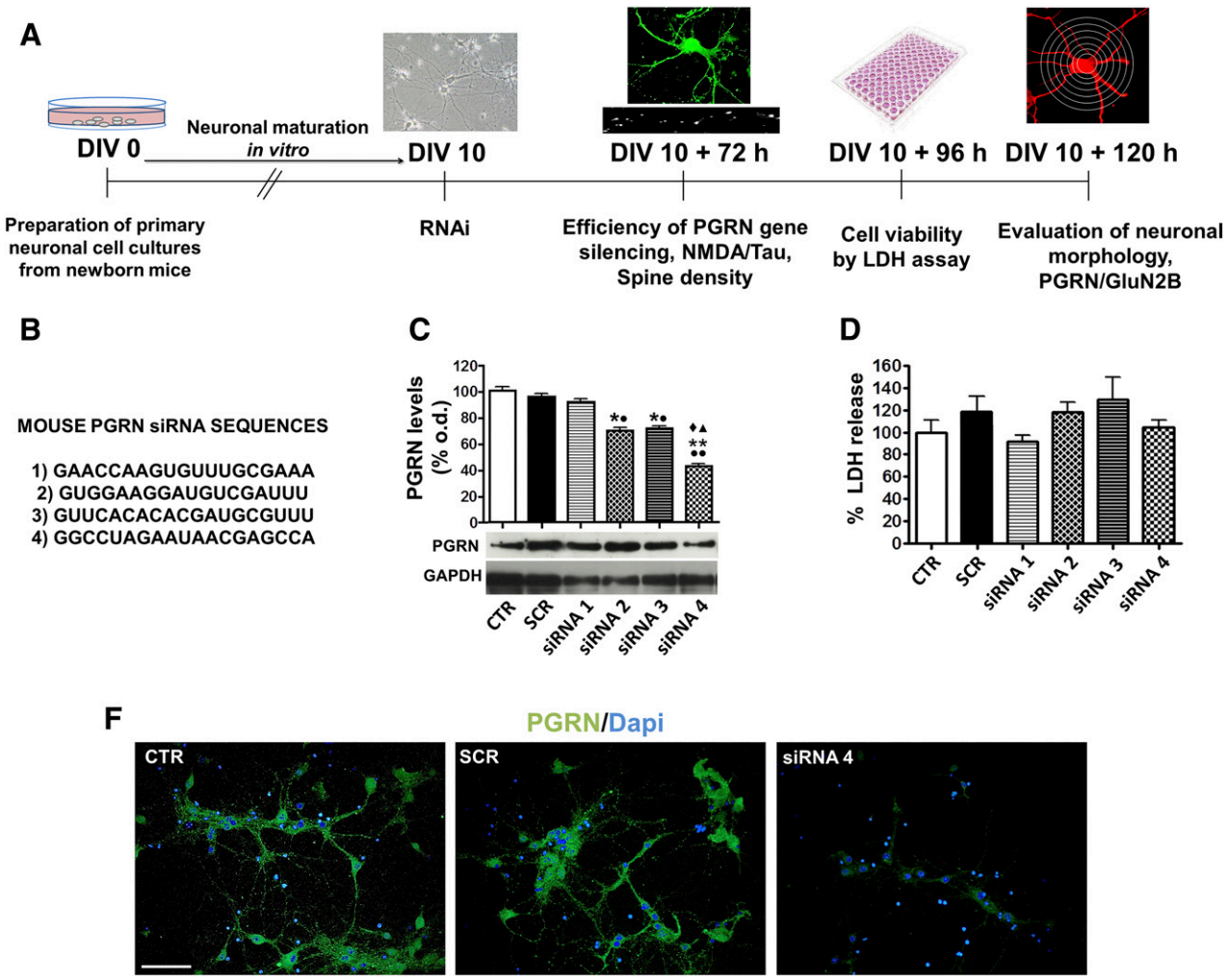

Fig. 3. Evaluation of PGRN gene silencing efficiency. (A) Schematic diagram showing the time-course of the study addressing the effect of PGRN gene silencing in primary cortical neurons. (B) siRNA sequences tested to induce PGRN gene silencing in mouse primary cortical neurons. (C) Histogram showing the efficiency of PGRN gene silencing evaluated as percentage decrease in protein levels in relation to control cells as measured by Western blot. Please note that siRNA sequence number 4 was able to induce the highest degree of PGRN gene silencing compared with both control (CTR) and SCR-treated neurons; $^{**}P < 0.01$ −60% vs. CTR, $\bullet\bullet P < 0.01$%–55% vs. SCR. This difference was also statistically significant against siRNA 1 ($\blacklozenge P < 0.01$) and siRNA 2 and 3 ($\blacktriangle P < 0.05$). Indeed, siRNA1 did not significantly reduce PGRN levels, and siRNA 2 and siRNA 3 induced only a modest although significant reduction in PGRN levels compared with either control or SCR-treated cells, respectively ($^{*}P < 0.05$ vs. CTR; $\bullet P < 0.01$ vs. SCR, one-way ANOVA + Newman-Keuls postcomparison test with $N = 3$ triplicates for each experimental condition analyzed. (D) Histogram showing the percentage LDH release in relation to control samples as a measure of cell viability and showing that siRNA sequence 4 did not significantly increase LDH release from primary neuronal cells compared with either control or SCR-treated cells (one-way ANOVA + Newman-Keuls postcomparison test with $N = 3$ triplicates for each experimental condition analyzed). (E) Representative photomicrographs showing fluorescence PGRN immunoreactivity in primary mouse cortical neurons in basal condition (CTR) after exposure to nonsilencing SCR RNA or siRNA4. Please note the decrease in PGRN immunopositivity in the cells exposed to siRNA4, which is indicative of the specificity of the PGRN signal and the efficiency of silencing of this specific siRNA. Scale bar, 100 μm.

viability assayed by LDH release assay at 96 hours (Fig. 3D). The reduction in PGRN by siRNA 4 was confirmed by immunocytochemical analysis (Fig. 3E).

PGRN Gene Silencing Reduces GluN2B-Containing NMDAR Density and Expression

To evaluate whether PGRN gene silencing could influence NMDA receptors we probed whether this could change the membrane levels and density of GluN2B-containing NMDA receptors. The choice to analyze GluN2B-containing NMDA receptors was mostly related to the fact that their expression and clustering in primary cortical neurons appears to be established from DIV 3, whereas GluN2A developmental expression and clustering are delayed and became detectable between DIV 12 and DIV 18 (Li et al., 1998; Mizuta et al., 1998; Desai et al., 2002). In line with these findings, we found that GluN2A was not detectable in primary cortical neurons at DIV 15 (Supplemental Fig. 1A). The levels of GluN1 and GluN2B in the membrane protein extracts were analyzed by Western blot (Fig. 4A). We found that PGRN gene silencing induced a statistically significant reduction in both GluN1 (** −22.8%; $P < 0.01$) and GluN2B levels (** −39%; $P < 0.01$), as indicated by the reduced density of the immunopositive bands compared with control neurons. Exposure to SCR RNA sequences did not alter GluN1 and GluN2B levels (Fig. 4A). Likewise, GluN1 and GluN2B levels were found to be reduced in total protein extracts produced from siRNA-exposed primary cortical neurons compared with either control or SCR RNA-treated cells (Supplemental Fig. 1B). We also probed whether silenced

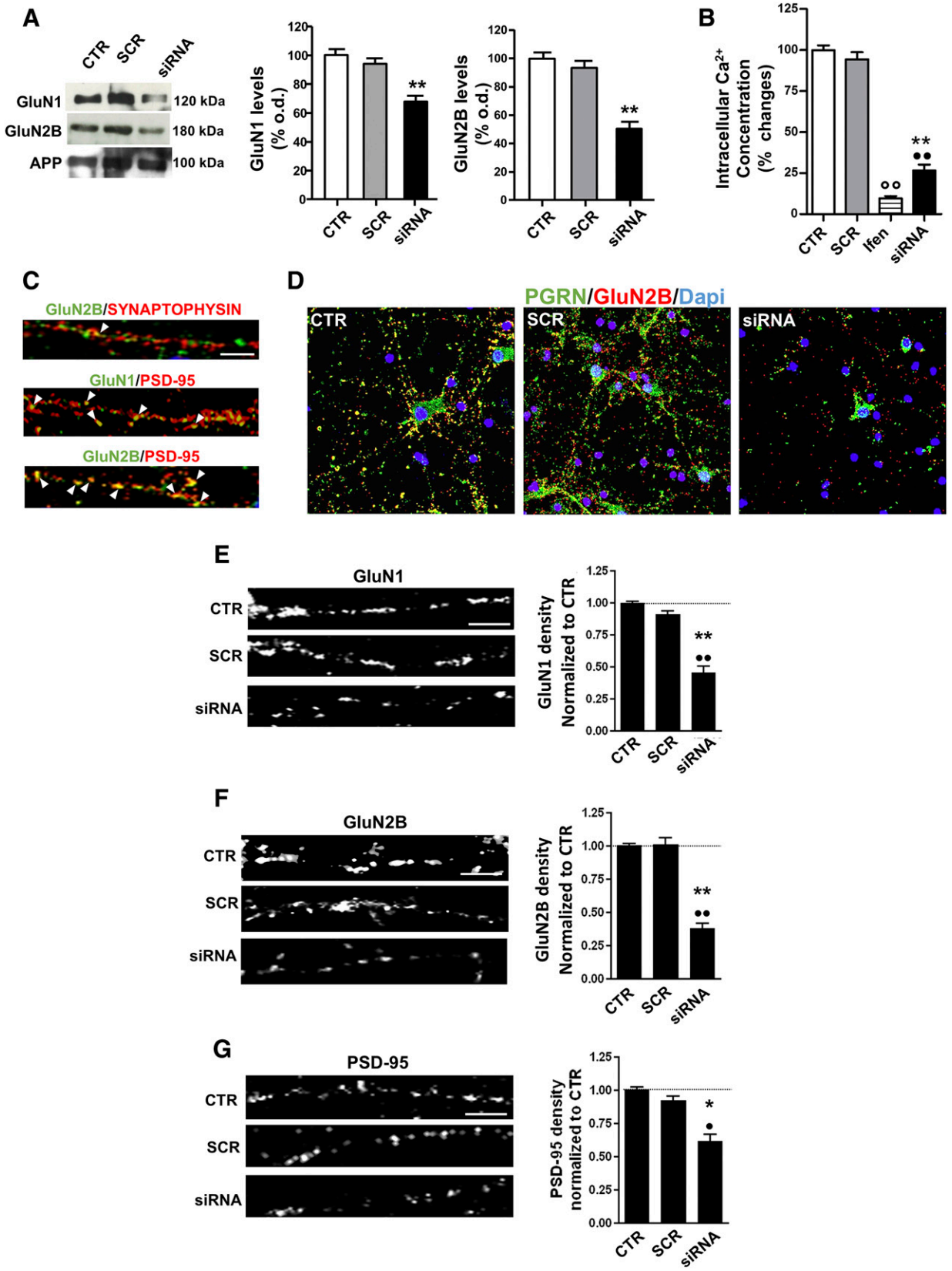

Fig. 4. GluN2B-containing NMDA levels and distribution in control, SCR-, and siRNA-exposed primary mouse cortical neurons at 72 hours from gene silencing. (A) Representative Western blot images showing GluN1, GluN2B, and amyloid precursor protein (APP)-immunopositive Western blot bands from membrane protein extracts of control (CTR), SCR-, or siRNA-exposed neurons are shown on the left. The histograms show the quantification of Western blot immunopositive bands (mean + S.D.) for GluN1 and GluN2B proteins when normalized against APP as a reference membrane protein. $^{**}P < 0.01$ vs. ctr, one-way ANOVA + Newman-Keuls postcomparison test ($N = 5$ triplicates for each experimental condition analyzed). (B) Histogram showing the percentage changes (mean % vs. CTR + S.D.) in intracellular Ca^{2+} concentration observed in control, SCR-, or siRNA-exposed cortical

neurons may display decreased activation of GluN2B-containing NMDA receptors after NMDA + glycine exposure. By using the GluN2B selective antagonist ifenprodil we found that NMDA + glycine-induced Ca^{2+} release from primary cortical neurons was GluN2B-dependent (Fig. 4B). Moreover, we observed that cells exposed to PGRN gene silencing showed a decreased Ca^{2+} overflow upon NMDA stimulation (Fig. 4B). We also evaluated whether PGRN gene silencing could decrease the levels of α-amino-3-hydroxy-5-methyl-4-isoxazolepropionic acid (AMPA) receptors in primary cortical neurons. We found that the cells that were exposed to siRNA did not exhibit a decrease in GluA1 or GluA2 levels (Supplemental Fig. 1C).

We investigated next the colocalization between NMDA receptors with either the presynaptic protein marker synaptophysin or the postsynaptic protein PSD-95 in primary control cortical neurons at DIV 10 (Fig. 4C). The results showed that GluN2B and GluN1 mostly colocalized with the postsynaptic marker PSD-95, whereas NR2B only showed a modest colocalization with synaptophysin, thus indicating that GluN2B-containing NMDA receptors were mostly localized at extrasynaptic sites (Fig. 4C). We then probed at 72 hours from gene silencing the density of GluN1, GluN2B, and PSD-95 ICC in neurons that were double-labeled with NMDA and PGRN to ensure that we could measure the changes in relation of PGRN levels (Fig. 4D). The densitometric analysis showed that cells that were exposed to PGRN gene silencing displayed a statistically significant reduction in density of GluN1 (Fig. 4E), GluN2B (Fig. 4F), and PSD-95 (Fig. 4G) compared with control or SCR-treated cells. Finally, since it has been previously described that PGRN depletion can cause a decrease in spine density (Petkau et al., 2012), we also assayed whether the decrease in NR1, NR2B, and PSD-95 might coincide with a reduction in dendritic spines. We found that at 72 hours from siRNA exposure primary neuronal cells showed a statistically significant reduction in spine density compared with either control ($P < 0.001$) or SCR RNA-treated cells ($P < 0.01$) (Supplemental Fig. 1D). These results support the conclusion that the decrease in GluN2B-containing NMDA receptors observed after PGRN depletion was associated with a reduction in spine density.

PGRN Gene Silencing Reduces Neuronal Arborization

Neuronal arborization was analyzed by Sholl analysis (Chen and Firestein, 2007; Kutzing et al., 2010) by evaluating the differences in the number of dendritic intersections between MAP-2-positive control, SCR-exposed and siRNA-exposed neurons at 120 hours from gene silencing. To assess whether GluN2B-containing NMDA receptor stimulation could be involved in the onset of the PGRN gene silencing–dependent decrease in neuronal arborization, we also analyzed siRNA-exposed cells that were subjected to acute stimulation with either NMDA + glycine or NMDA + glycine following ifenprodil pretreatment. We found that cells exposed to PGRN gene silencing showed a statistically significant decrease in dendritic intersections (Fig. 5A) at 60, 90, 120, and 150 μm from the soma (Fig. 5B). To corroborate the specificity of the effect of PGRN gene silencing on neuronal arborization, we compared the effect of siRNA1, siRNA2, siRNA3, and siRNA4 on this parameter. In line with the data deriving from the evaluation of the gene silencing efficiency of these sequences, we found that siRNA2 and siRNA3 induced a modest increase in neuronal arborization, whereas siRNA4 significantly reduced the number of intersections at 30, 60, 90, 120, and 150 μm from the soma compared with siRNA1 (Supplemental Fig. 2, A and B). These observations were corroborated by data showing that the efficiency rate of PGRN gene silencing achieved by using the different siRNA sequences was inversely correlated with the total number of intersections counted for siRNA1, siRNA2, siRNA3, or siRNA4 (Supplemental Fig. 2C).

We then wanted to probe the effect of NMDA stimulation on neuronal arborization in siRNA4-exposed cells. Of note, an acute stimulation of cortical neurons with NMDA + glycine at 24 hours from gene silencing could prevent the effect of PGRN gene silencing on neuronal arborization. Indeed, the NMDA + glycine treated PGRN-silenced neurons showed a weaker, although significant difference in the number of dendritic intersections only at 60 and 90 μm from the soma compared with siRNA-exposed cells. Of note, a pretreatment with the GluN2B selective antagonist ifenprodil before the acute stimulation with NMDA + glycine in siRNA-exposed cells was able to significantly prevent the effect of NMDA stimulation on neuronal arborization in the cells exposed to PGRN gene silencing. Finally, we evaluated the persistence of GluN2B decrease in MAP-2 positive cells at 120 hours from gene silencing to ensure they effectively displayed GluN2B reduction. As shown in Fig. 5C we observed a decrease in GluN2B in the siRNA-exposed MAP-2-positive cells but not in control or SCR-treated neurons.

PGRN Gene Silencing Affects NMDA Receptor-Dependent Tau Phosphorylation. To evaluate whether PGRN gene silencing could modulate NMDA-dependent tau phosphorylation, we assayed by Western blot tau phosphorylation of Ser 262, 396, and 404 normalized against total tau levels probed by using the tau 46 antibody (Fig. 6A).

We found that PGRN gene silencing significantly reduced the levels of tau phosphorylation in cortical neurons exposed to

neurons at 72 hours from RNAi after NMDA + glycine stimulation. PGRN-deficient cells show a statistically significant reduction in NMDA-induced Ca^{2+} overflow compared with both control or SCR-treated neurons (**$P < 0.01$ vs. CTR; ••$P < 0.01$ vs. SCR, one-way ANOVA + Newman-Keuls postcomparison test with $N = 5$ triplicates for each experimental condition analyzed). (C) Representative photomicrographs showing GluN2B/synaptophysin, GluN1/PSD-95, and GluN2B/PSD-95 double-labeling in primary cortical neurons in basal condition. Please note that GluN2B mis-localizes with the presynaptic marker synaptophysin at the same time it colocalizes with the postsynaptic protein PSD-95. Scale bars, upper panel 40 μm, lower panel 20 μm. (D) Representative photomicrographs showing PGRN/GluN2B double fluorescence immunolabeling in control SCR- or siRNA-exposed primary mouse cortical neurons. Please note the decrease in both proteins in the neurons exposed to siRNA. Scale bar, 90 μm. (E) GluN1 subunit distribution in primary cortical neurons in the different experimental conditions analyzed at 72 hours from gene silencing. Please note the statistically significant reduction in GluN1 density along neuronal processes in the siRNA-exposed cells compared with both control or SCR-treated neurons that is evident in the histogram showing the densitometric analysis (**$P < 0.01$ vs. CTR and ••$P < 0.01$ vs. SCR, one-way ANOVA + Newman-Keuls, $N = 10$ triplicates for each experimental condition analyzed). Scale bar, 20 μm. (F) Density of GluN2B along neuronal processes. Please note the statistically significant decrease in the cells exposed to PGRN gene silencing compared with control or SCR-exposed neurons. (**$P < 0.01$ vs. CTR and ••$P < 0.01$ vs. SCR, one-way ANOVA + Newman-Keuls, $N = 10$ triplicates for each experimental condition analyzed). Scale bar, 20 μm. (G) PSD-95 distribution. Please note the significant decrease in PSD-95 density in the cells exposed to PGRN gene silencing compared with either CTR or SCR-treated cells (*$P < 0.05$ vs. CTR and •$P < 0.05$ vs. SCR, one-way ANOVA + Newman-Keuls, $N = 10$ triplicates for each experimental condition analyzed). Scale bar, 20 μm.

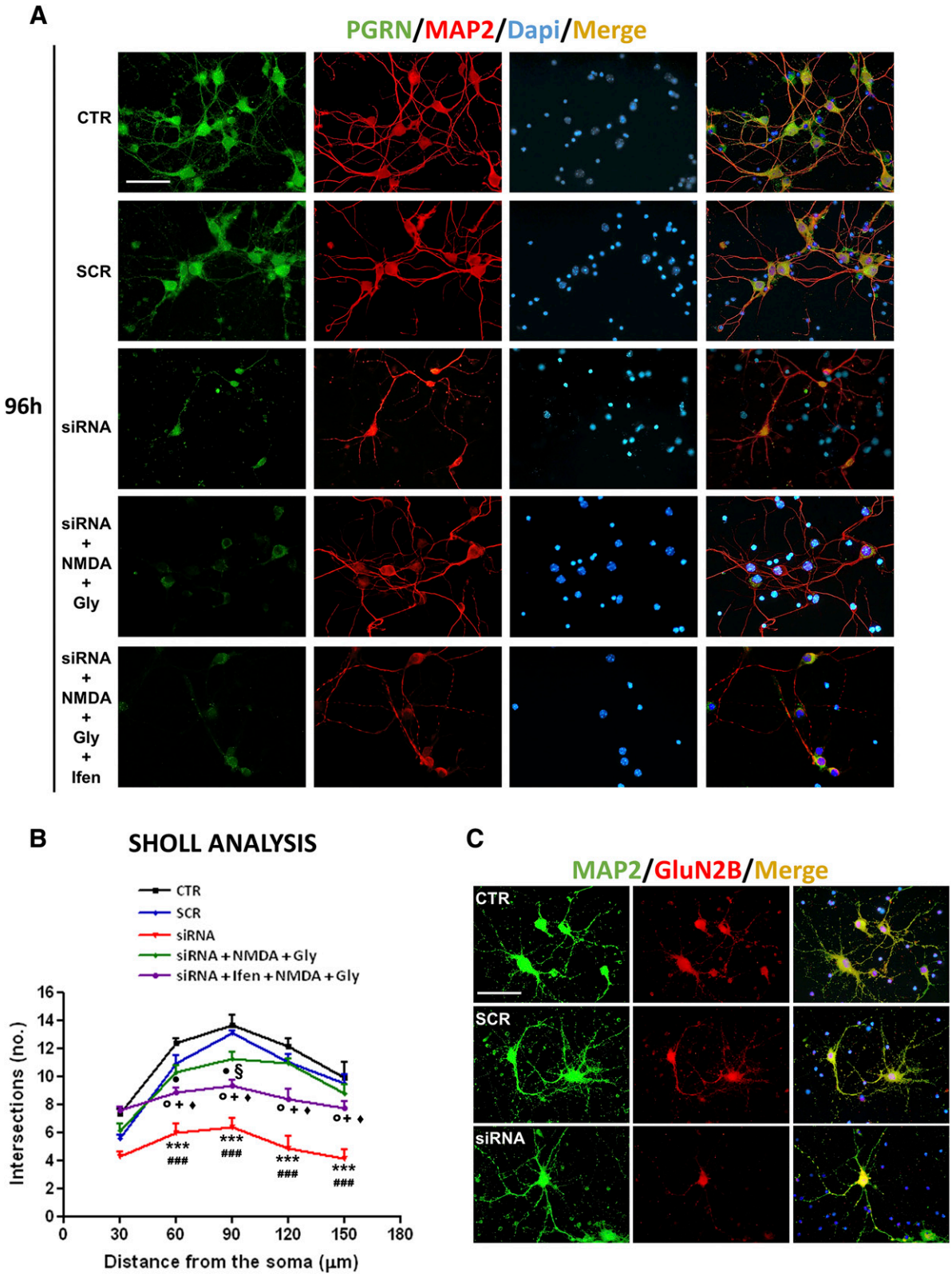

Fig. 5. Analysis of MAP-2-positive cell arborization in primary cortical neurons. (A) Immunofluorescence images showing PGRN/MAP-2 double-labeling in CTR, SCR-, and siRNA-exposed cells. A fraction of siRNA exposed cells was subjected to NMDA + glycine or ifenprodil (ifen) + NMDA + glycine treatment. Please note that siRNA-exposed neurons show a decrease in neuronal arborization compared with CTR or SCR-treated neurons. Silenced neurons that were treated with NMDA + glycine appeared morphologically similar to controls. However, cells subjected to ifenprodil pretreatment prior NMDA + glycine stimulation were similar to siRNA-exposed neurons. Scale bar, 90 μm. (B) The graph shows the results of the Scholl analysis. Please note that although siRNA-exposed neurons showed a statistically significant decrease in the number of intersections compared with both CTR and SCR-exposed neurons, in the silenced cells that were subjected to the acute NMDA + glycine (Gly) treatment the arborization was not decreased. The protective effect of NMDA + Gly stimulation was prevented by treatment with the GluN2B

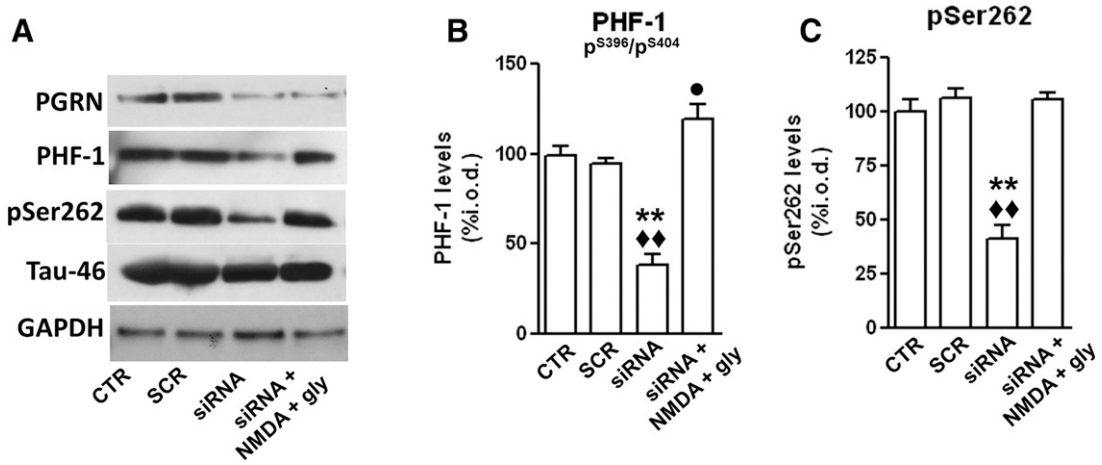

Fig. 6. PGRN gene silencing reduces NMDA-mediated tau phosphorylation. (A) Representative immunoblotting showing PGRN, PHF-1 (serine 396/404), serine 262 phosphorylated, and total (tau 46-positive) tau. Glyceraldehyde-3-phosphate dehydrogenase–positive bands are reported as a control for equal loading. (B) Histogram showing the quantification of PHF-1-immunopositive bands when normalized vs. tau 46-immunopositive bands. Please note the statistically significant decrease in PHF-1-positive tau in siRNA exposed neurons compared with control (**$P < 0.01$) and SCR-exposed (♦♦$P < 0.01$ vs. SCR) cells. This effect was prevented in NMDA + glycine–treated cells that showed a significant increase of tau phosphorylation compared with SCR-exposed neurons (●$P < 0.05$ one-way ANOVA + Newman-Keuls postcomparison test). (C) NMDA treatment could also prevent the statistically significant reduction in serine 262 tau phosphorylation induced by PGRN gene silencing (**$P < 0.01$ vs. CTR; ♦♦$P < 0.01$ vs. SCR, one-way ANOVA + Newman-Keuls postcomparison test).

siRNA compared with control or SCR RNA-treated cells. However, the acute treatment with NMDA + glycine could prevent the reduction in tau phosphorylation in siRNA-exposed neurons, indicating that the abatement of tau phosphorylation was related to the decrease in NMDA receptor levels and activity observed in the cells with PGRN gene silencing.

Discussion

Collectively, our results indicate that a partial drop of PGRN affects GluN2B-containing NMDA receptor density, tau phosphorylation as well as dendritic arborization in primary mouse cortical neurons. In particular, we found that haploinsufficiency-like PGRN depletion, achieved by RNAi, could reduce GluN1 and GluN2B membrane levels and density at 72 hours from gene silencing. These alterations were associated with a reduction in spine density and NMDA receptor-mediated Ca^{2+}-influx in primary cortical neurons, followed by a decrease in neuronal arborization 96 hours after RNAi. Notably, we found that the decrease in neuronal arborization induced by PGRN gene silencing was prevented by NMDA receptor stimulation, whose effect was in turn reversed by the GluN2B selective antagonist ifenprodil, thereby supporting the existence of a causative link between these phenomena. Indeed, this evidence suggests that the decrease in GluN2B-containing NMDA receptors could mediate the negative effect of PGRN abatement on neuronal trophism. To date, in line with our data, it has been found that, although GluN2B is not essential for dendrite growth and branching, its knockdown is characterized by a decrease in neuronal spine density and the number of apical dendrites (Espinosa et al., 2009), thus suggesting that GluN2B action is relevant for dendrite patterning. In primary cortical neurons in culture at DIV 10, NMDA activity at excitatory synapses is assured by the coupling of GluN1 and GluN2B that can cluster at both synaptic and extrasynaptic sites, with only a very small fraction of synaptic NMDA receptors containing the GluN2A subunit (Li et al., 1998). These findings indicate that NMDA-dependent regulation of primary cortical neurons is strictly dependent on GluN2B-containing NMDA receptors. In line with this hypothesis and with our findings, inhibition of primary cortical neurons has been found to be associated with dendrite degeneration and reduced ERK1/2 kinase activation in primary neurons (Chernova et al., 2007).

Our results also showed that PGRN gene silencing could decrease GluN2B-containing NMDA receptor-mediated tau phosphorylation at Ser 262 and PHF-1 sites. This observation suggests that PGRN haploinsufficiency, by reducing GluN2B-containing NMDA receptor signaling, can affect the structural plasticity of cortical neurons by modulating the ability of tau to interact with microtubules. Indeed, as a result of reduced tau phosphorylation, microtubular networks could be impaired by stiffness, and parallel synapse formation could be hampered, thus generating the loss in neuronal connectivity typical for FTLD. Although further studies are needed to probe this hypothesis, it is well recognized that interaction of tau with microtubules is essential for the proper maintenance of neuronal structural plasticity and for the transport of synaptic cargoes along microtubules. The loss of efficient interaction of tau with microtubules derived from its hyperphosphorylation is implicated in the onset of several neurodegenerative diseases affecting cortical regions, including familial FTLD (Spillantini and Goedert, 2013). Proper tau activity is thus crucial for cortical neuron function and homeostasis, and subtle changes in the post-translational modifications that drive tau function could severely

selective antagonist ifenprodil (Ifen). •$P < 0.05$ vs. CTR, §$P < 0.05$ vs. SCR, ○$P < 0.05$ vs. CTR, ♦$P < 0.05$ vs. SCR, + $P < 0.05$ vs. siRNA, ***$P <$ 0.001 vs. CTR, ###$P < 0.001$ vs. SCR; two-way ANOVA + Bonferroni's postcomparison test, $N = 6$ triplicates for each experimental condition analyzed. (C) Representative photomicrographs showing MAP-2/GluNB double-labeling in control, SCR, or siRNA-exposed primary cortical neurons at 96 hours from RNAi. Please note the lower GluN2B-immunopositive signal in the siRNA exposed cells. Scale bar, 90 μm.

impinge on cortical neuron resilience. In this scenario, tau hyperphosphorylation, which generates neurofibrillary tangles in Microtubule-Associated Protein Tau-associated FTLD, and tau hypophosphorylation, which results from PGRN reduction in FTLD with PGRN mutations, could be two opposite mechanisms that drive neuronal cells toward degeneration by compromising tau-microtubular interaction. Our results support the conclusion that the reduced activity of NMDA receptors deriving from low PGRN levels could pivotally control the capacity of tau to interact with microtubules in FTLD with PGRN mutations. Notably, several previous research reports have described the occurrence of NMDA receptor-mediated tau phosphorylation in neuronal cells (Zhou et al., 2009; Sava et al., 2012), suggesting that this process could be part of a physiologic intracellular signaling cascade regulating synaptic NMDA receptor-dependent transmission during structural plasticity changes. In particular, NMDA receptors can increase the phosphorylation of tau on specific sites that mediate its interaction with synaptic proteins. Moreover, the phosphorylation of tau controls the interaction of tau with the postsynaptic PSD-95-Fyn-NMDA receptor complex, which regulates GluN2B-containing NMDA-dependent synaptic plasticity, suggesting that physiologically occurring phosphorylation of tau could serve as a regulatory mechanism to prevent NMDA receptor overexcitation (Mondragon-Rodriguez et al., 2012). These findings, coupled to our results, hint that a decrease in PGRN increases neuronal vulnerability by leading to a reduction in GluN2B-containing NMDA receptors, which in turn affects the rate of tau phosphorylation and might perturb the ability of neuronal cells to easily display structural plasticity changes. Structural changes occur in the brain throughout life, including the generation of new neurons and other brain cells and connections between and among neurons, and structural plasticity provides the mechanism for the brain to repair itself (Gage, 2004). In addition, subtle changes in functional plasticity in brain cortical areas can contribute to behavioral impairments in the absence of significant pathology (Burke and Barnes, 2006). This implies that in PGRN mutation carriers, cortical neurons holding reduced PGRN levels may present a lower ability to display structural plasticity changes. This phenomenon may also significantly decrease the resilience of these cells to aging and stressors.

Consistent with our conclusions are recent reports that PGRN-deficient mice display reduced synaptic connectivity and plasticity impairment occurring before neuropathological abnormalities (Petkau et al., 2012). Moreover, PGRN deficiency reduces synaptic pruning in the thalamus by dysregulating microglial cells (Lui et al., 2016). Our findings show that the PGRN-deficiency–related decrease in neuronal arborization is attributable to a decrease in NR2B-containing NMDA receptors that is paralleled by a decrease in spine density. This evidence is in tune with previous findings showing that, although PGRN reduction can enhance transmission at individual synapses, it decreases gross neuronal connectivity (Tapia et al., 2011), and confirms that important neuronal plasticity changes occur in the early stages of disease. Remarkably, both NMDA receptor activity and tau phosphorylation have been found to be highly involved in the control of microtubule dynamic changes during neuronal structural plasticity (Caceres and Kosik, 1990; Knops et al., 1991; Biernat and Mandelkow, 1999; Dawson et al., 2001).

Worthy of note, a recent finding indicates that PGRN reduction is associated with increased tau phosphorylation in P301L transgenic mice (Hosokawa et al., 2015). Although in part these observations are not in agreement with our results, which indicate that a decrease in PGRN reduces tau phosphorylation, it is feasible that other mechanisms may be involved in the opposite phenomenon in the transgenic P301L tau model. This is supported by the fact that PGRN-deficient mice do not show tau hyperphosphorylation (Hosokawa et al., 2015). In addition, we cannot exclude that a partial reduction in PGRN resulting in the case of haploinsufficiency may affect neuronal homeostasis in a manner completely different from the complete absence of the protein, as supported by the different pathologic phenotypes described for PGRN-knockout and PGRN-insufficient mice (Yin et al., 2010; Martens et al., 2012; Petkau et al., 2012; Filiano et al., 2013; Arrant et al., 2015). Data in human cerebrospinal fluids further support our experimental evidence, as we previously described that tau phosphorylation is increased in Alzheimer's disease patients and in FTLD patients compared with controls but not in FTLD patients carrying a GRN mutation that causes progranulin haploinsufficiency (Carecchio et al., 2011).

The results of this study indicate that an haploinsufficiency-like decrease in PGRN can reduce the density and activity of GluN2B-containing NMDA receptors. This phenomenon is associated with a reduction in NMDA receptor-mediated tau phosphorylation as well as a loss of neuronal dendritic arborization, which is reversible by an acute GluN2B-containing NMDA receptor stimulation at 24 hours from gene silencing. These findings support the conclusions that GluN2B-containing NMDA receptors could be crucial mediators for the control of PGRN-dependent cortical neuron neurotrophism.

Collectively, these observations suggest that an aberrant regulation of GluN2B-containing NMDA receptors resulting from PGRN loss of function mutations could impinge on cortical neuron resilience by perturbing their ability to display structural plasticity changes. The resulting progressive decline of neuronal trophism could probably initiate neurodegeneration in FTLD with GRN mutations.

These observations have relevant implications for understanding the molecular mechanisms underlying the onset of FTLD.

Acknowledgments

The authors are grateful to Alessandro Barbon for providing the GluN2A, GluA1, and GluA2 antibodies.

Authorship Contributions

Participated in research design: Bellucci, Spano, Zaltieri.

Conducted experiments: Bellucci, Longhena, Zaltieri, Grigoletto, Faustini, La Via.

Performed data analysis: Longhena, Zaltieri, Grigoletto.

Wrote or contributed to the writing of the manuscript: Bellucci, Longhena, Ghidoni, Benussi, Spano, Missale.

References

Arendt T, Stieler J, and Holzer M (2015) Brain hypometabolism triggers PHF-like phosphorylation of tau, a major hallmark of Alzheimer's disease pathology. *J Neural Transm (Vienna)* **122**:531–539.

Arrant AE, Patel AR, and Roberson ED (2015) Effects of exercise on progranulin levels and gliosis in progranulin-insufficient mice. *eNeuro* **2**:1–12 DOI: https://doi.org/10.1523/ENEURO.0061-14.2015.

Baker M, Mackenzie IR, Pickering-Brown SM, Gass J, Rademakers R, Lindholm C, Snowden J, Adamson J, Sadovnick AD, Rollinson S, et al. (2006) Mutations in progranulin cause tau-negative frontotemporal dementia linked to chromosome 17. *Nature* **442**:916–919.

Benussi L, Ciani M, Tonoli E, Morbin M, Palamara L, Albani D, Fusco F, Forloni G, Glionna M, Baco M, et al. (2016) Loss of exosomes in progranulin-associated frontotemporal dementia. *Neurobiol Aging* **40**:41–49.

Biernat J and Mandelkow EM (1999) The development of cell processes induced by tau protein requires phosphorylation of serine 262 and 356 in the repeat domain and is inhibited by phosphorylation in the proline-rich domains. *Mol Biol Cell* **10**:727–740.

Borroni B, Alberici A, Cercignani M, Premi E, Serra L, Cerini C, Cosseddu M, Pettenati C, Turla M, Archetti S, et al. (2012) Granulin mutation drives brain damage and reorganization from preclinical to symptomatic FTLD. *Neurobiol Aging* **33**:2506–2520.
Bozzali M, Battistoni V, Premi E, Alberici A, Giulietti G, Archetti S, Turla M, Gasparotti R, Cercignani M, Padovani A, et al. (2013) Structural brain signature of FTLD driven by Granulin mutation. *J Alzheimers Dis* **33**:483–494.
Burke SN and Barnes CA (2006) Neural plasticity in the ageing brain. *Nat Rev Neurosci* **7**:30–40.
Caceres A and Kosik KS (1990) Inhibition of neurite polarity by tau antisense oligonucleotides in primary cerebellar neurons. *Nature* **343**:461–463.
Carecchio M, Fenoglio C, Cortini F, Comi C, Benussi L, Ghidoni R, Borroni B, De Riz M, Serpente M, Cantoni C, et al. (2011) Cerebrospinal fluid biomarkers in Progranulin mutations carriers. *J Alzheimers Dis* **27**:781–790.
Carpenter-Hyland EP and Chandler LJ (2007) Adaptive plasticity of NMDA receptors and dendritic spines: implications for enhanced vulnerability of the adolescent brain to alcohol addiction. *Pharmacol Biochem Behav* **86**:200–208.
Chen H and Firestein BL (2007) RhoA regulates dendrite branching in hippocampal neurons by decreasing cypin protein levels. *J Neurosci* **27**:8378–8386.
Chernova T, Steinert JR, Guerin CJ, Nicotera P, Forsythe ID, and Smith AG (2007) Neurite degeneration induced by heme deficiency mediated via inhibition of NMDA receptor-dependent extracellular signal-regulated kinase 1/2 activation. *J Neurosci* **27**:8475–8485.
Chitramuthu BP, Baranowski DC, Kay DG, Bateman A, and Bennett HP (2010) Progranulin modulates zebrafish motoneuron development in vivo and rescues truncation defects associated with knockdown of Survival motor neuron 1. *Mol Neurodegener* **5**:41.
Cruts M, Gijselinck I, van der Zee J, Engelborghs S, Wils H, Pirici D, Rademakers R, Vandenberghe R, Dermaut B, Martin JJ, et al. (2006) Null mutations in progranulin cause ubiquitin-positive frontotemporal dementia linked to chromosome 17q21. *Nature* **442**:920–924.
Dawson HN, Ferreira A, Eyster MV, Ghoshal N, Binder LI, and Vitek MP (2001) Inhibition of neuronal maturation in primary hippocampal neurons from tau deficient mice. *J Cell Sci* **114**:1179–1187.
Desai A, Turetsky D, Vasudevan K, and Buonanno A (2002) Analysis of transcriptional regulatory sequences of the N-methyl-D-aspartate receptor 2A subunit gene in cultured cortical neurons and transgenic mice. *J Biol Chem* **277**:46374–46384.
El Gaamouch F, Buisson A, Moustié O, Lemieux M, Labrecque S, Bontempi B, De Koninck P, and Nicole O (2012) Interaction between αCaMKII and GluN2B controls ERK-dependent plasticity. *J Neurosci* **32**:10767–10779.
Espinosa JS, Wheeler DG, Tsien RW, and Luo L (2009) Uncoupling dendrite growth and patterning: single-cell knockout analysis of NMDA receptor 2B. *Neuron* **62**:205–217.
Filiano AJ, Martens LH, Young AH, Warmus BA, Zhou P, Diaz-Ramirez G, Jiao J, Zhang Z, Huang EJ, Gao FB, et al. (2013) Dissociation of frontotemporal dementia-related deficits and neuroinflammation in progranulin haploinsufficient mice. *J Neurosci* **33**:5352–5361.
Finch N, Baker M, Crook R, Swanson K, Kuntz K, Surtees R, Bisceglio G, Rovelet-Lecrux A, Boeve B, Petersen RC, et al. (2009) Plasma progranulin levels predict progranulin mutation status in frontotemporal dementia patients and asymptomatic family members. *Brain* **132**:583–591.
Gage FH (2004) Structural plasticity of the adult brain. *Dialogues Clin Neurosci* **6**: 135–141.
Ghidoni R, Benussi L, Glionna M, Franzoni M, and Binetti G (2008) Low plasma progranulin levels predict progranulin mutations in frontotemporal lobar degeneration. *Neurology* **71**:1235–1239.
Ghidoni R, Paterlini A, Albertini V, Binetti G, and Benussi L (2012) Losing protein in the brain: the case of progranulin. *Brain Res* **1476**:172–182.
Gijselinck I, van der Zee J, Engelborghs S, Goossens D, Peeters K, Mattheijssens M, Corsmit E, Del-Favero J, De Deyn PP, Van Broeckhoven C, et al. (2008) Progranulin locus deletion in frontotemporal dementia. *Hum Mutat* **29**:53–58.
Hosokawa M, Arai T, Masuda-Suzukake M, Kondo H, Matsuwaki T, Nishihara M, Hasegawa M, and Akiyama H (2015) Progranulin reduction is associated with increased tau phosphorylation in P301L tau transgenic mice. *J Neuropathol Exp Neurol* **74**:158–165.
Jian J, Konopka J, and Liu C (2013) Insights into the role of progranulin in immunity, infection, and inflammation. *J Leukoc Biol* **93**:199–208.
Knops J, Kosik KS, Lee G, Pardee JD, Cohen-Gould L, and McConlogue L (1991) Overexpression of tau in a nonneuronal cell induces long cellular processes. *J Cell Biol* **114**:725–733.
Kutzing MK, Langhammer CG, Luo V, Lakdawala H, and Firestein BL (2010) Automated Sholl analysis of digitized neuronal morphology at multiple scales. *J Vis Exp* **45**: e2354.
Laird AS, Van Hoecke A, De Muynck L, Timmers M, Van den Bosch L, Van Damme P, and Robberecht W (2010) Progranulin is neurotrophic in vivo and protects against a mutant TDP-43 induced axonopathy. *PLoS One* **5**:e13368.
Laulagnier K, Javalet C, Hemming FJ, and Sadoul R (2017) Purification and analysis of exosomes released by mature cortical neurons following synaptic activation. *Methods Mol Biol* **1545**:129–138.
Laurier-Laurin ME, De Montigny A, Attiori Essis S, Cyr M, and Massicotte G (2014) Blockade of lysosomal acid ceramidase induces GluN2B-dependent tau phosphorylation in rat hippocampal slices. *Neural Plast* **2014**:196812.
Li JH, Wang YH, Wolfe BB, Krueger KE, Corsi L, Stocca G, and Vicini S (1998) Developmental changes in localization of NMDA receptor subunits in primary cultures of cortical neurons. *Eur J Neurosci* **10**:1704–1715.
Lui H, Zhang J, Makinson SR, Cahill MK, Kelley KW, Huang HY, Shang Y, Oldham MC, Martens LH, Gao F, et al. (2016) Progranulin deficiency promotes circuit-specific synaptic pruning by microglia via complement activation. *Cell* **165**:921–935.
Martens LH, Zhang J, Barmada SJ, Zhou P, Kamiya S, Sun B, Min SW, Gan L, Finkbeiner S, Huang EJ, et al. (2012) Progranulin deficiency promotes neuroinflammation and neuron loss following toxin-induced injury. *J Clin Invest* **122**:3955–3959.
McKhann GM, Albert MS, Grossman M, Miller B, Dickson D, and Trojanowski JQ; Work Group on Frontotemporal Dementia and Pick's Disease (2001) Clinical and pathological diagnosis of frontotemporal dementia: report of the Work Group on Frontotemporal Dementia and Pick's Disease. *Arch Neurol* **58**:1803–1809.
Mizuta I, Katayama M, Watanabe M, Mishina M, and Ishii K (1998) Developmental expression of NMDA receptor subunits and the emergence of glutamate neurotoxicity in primary cultures of murine cerebral cortical neurons. *Cell Mol Life Sci* **54**:721–725.
Mondragón-Rodríguez S, Trillaud-Doppia E, Dudilot A, Bourgeois C, Lauzon M, Leclerc N, and Boehm J (2012) Interaction of endogenous tau protein with synaptic proteins is regulated by N-methyl-D-aspartate receptor-dependent tau phosphorylation. *J Biol Chem* **287**:32040–32053.
Mony L, Kew JN, Gunthorpe MJ, and Paoletti P (2009) Allosteric modulators of NR2B-containing NMDA receptors: molecular mechanisms and therapeutic potential. *Br J Pharmacol* **157**:1301–1317.
Moretti DV, Benussi L, Fostinelli S, Ciani M, Binetti G, and Ghidoni R (2016) Progranulin mutations affects brain oscillatory activity in fronto-temporal dementia. *Front Aging Neurosci* **8**:35.
Navarria L, et al. (2015) Alpha-synuclein modulates NR2B-containing NMDA receptors and decreases their levels after rotenone exposure. *Neurochem Int* **85-86**:14–23.
Petkau TL, Hill A, and Leavitt BR (2016) Core neuropathological abnormalities in progranulin-deficient mice are penetrant on multiple genetic backgrounds. *Neuroscience* **315**:175–195.
Petkau TL and Leavitt BR (2014) Progranulin in neurodegenerative disease. *Trends Neurosci* **37**:388–398.
Petkau TL, Neal SJ, Milnerwood A, Mew A, Hill AM, Orban P, Gregg J, Lu G, Feldman HH, Mackenzie IR, et al. (2012) Synaptic dysfunction in progranulin-deficient mice. *Neurobiol Dis* **45**:711–722.
Petkau TL, Neal SJ, Orban PC, MacDonald JL, Hill AM, Lu G, Feldman HH, Mackenzie IR, and Leavitt BR (2010) Progranulin expression in the developing and adult murine brain. *J Comp Neurol* **518**:3931–3947.
Pievani M, Paternicò D, Benussi L, Binetti G, Orlandini A, Cobelli M, Magnaldi S, Ghidoni R, and Frisoni GB (2014) Pattern of structural and functional brain abnormalities in asymptomatic granulin mutation carriers. *Alzheimers Dement* **10** (Suppl 5)S354–S363, 363.e1.
Rohrer JD, Geser F, Zhou J, Gennatas ED, Sidhu M, Trojanowski JQ, Dearmond SJ, Miller BL, and Seeley WW (2010) TDP-43 subtypes are associated with distinct atrophy patterns in frontotemporal dementia. *Neurology* **75**:2204–2211.
Rohrer JD, Nicholas JM, Cash DM, van Swieten J, Dopper E, Jiskoot L, van Minkelen R, Rombouts SA, Cardoso MJ, Clegg S, et al. (2015) Presymptomatic cognitive and neuroanatomical changes in genetic frontotemporal dementia in the Genetic Frontotemporal dementia Initiative (GENFI) study: a cross-sectional analysis. *Lancet Neurol* **14**:253–262.
Rohrer JD, Warren JD, Fox NC, and Rossor MN (2013) Presymptomatic studies in genetic frontotemporal dementia. *Rev Neurol (Paris)* **169**:820–824.
Ryan CL, Baranowski DC, Chitramuthu BP, Malik S, Li Z, Cao M, Minotti S, Durham HD, Kay DG, Shaw CA, et al. (2009) Progranulin is expressed within motor neurons and promotes neuronal cell survival. *BMC Neurosci* **10**:130.
Sava A, Formaggio E, Carignani C, Andreetta F, Bettini E, and Griffante C (2012) NMDA-induced ERK signalling is mediated by NR2B subunit in rat cortical neurons and switches from positive to negative depending on stage of development. *Neuropharmacology* **62**:925–932.
Skoglund L, Matsui T, Freeman SH, Wallin A, Blom ES, Frosch MP, Growdon JH, Hyman BT, Lannfelt L, Ingelsson M, et al. (2011) Novel progranulin mutation detected in 2 patients with FTLD. *Alzheimer Dis Assoc Disord* **25**:173–178.
Sleegers K, Brouwers N, Van Damme P, Engelborghs S, Gijselinck I, van der Zee J, Peeters K, Mattheijssens M, Cruts M, Vandenberghe R, et al. (2009) Serum biomarker for progranulin-associated frontotemporal lobar degeneration. *Ann Neurol* **65**:603–609.
Spillantini MG and Goedert M (2013) Tau pathology and neurodegeneration. *Lancet Neurol* **12**:609–622.
Stein IS, Gray JA, and Zito K (2015) Non-ionotropic NMDA receptor signaling drives activity-induced dendritic spine shrinkage. *J Neurosci* **35**:12303–12308.
Tackenberg C, Grinschgl S, Trutzel A, Santuccione AC, Frey MC, Konietzko U, Grimm J, Brandt R, and Nitsch RM (2013) NMDA receptor subunit composition determines beta-amyloid-induced neurodegeneration and synaptic loss. *Cell Death Dis* **4**:e608.
Tapia L, Milnerwood A, Guo A, Mills F, Yoshida E, Vasuta C, Mackenzie IR, Raymond L, Cynader M, Jia W, et al. (2011) Progranulin deficiency decreases gross neural connectivity but enhances transmission at individual synapses. *J Neurosci* **31**:11126–11132.
Van Damme P, Van Hoecke A, Lambrechts D, Vanacker P, Bogaert E, van Swieten J, Carmeliet P, Van Den Bosch L, and Robberecht W (2008) Progranulin functions as a neurotrophic factor to regulate neurite outgrowth and enhance neuronal survival. *J Cell Biol* **181**:37–41.
Whitwell JL, Jack CR, Jr, Baker M, Rademakers R, Adamson J, Boeve BF, Knopman DS, Parisi JF, Petersen RC, Dickson DW, et al. (2007) Voxel-based morphometry in frontotemporal lobar degeneration with ubiquitin-positive inclusions with and without progranulin mutations. *Arch Neurol* **64**:371–376.
Williams JM, Guévremont D, Kennard JT, Mason-Parker SE, Tate WP, and Abraham WC (2003) Long-term regulation of N-methyl-D-aspartate receptor subunits and associated synaptic proteins following hippocampal synaptic plasticity. *Neuroscience* **118**:1003–1013.
Wyllie DJ, Livesey MR, and Hardingham GE (2013) Influence of GluN2 subunit identity on NMDA receptor function. *Neuropharmacology* **74**:4–17.
Yin F, Banerjee R, Thomas B, Zhou P, Qian L, Jia T, Ma X, Ma Y, Iadecola C, Beal MF, et al. (2010) Exaggerated inflammation, impaired host defense, and neuropathology in progranulin-deficient mice. *J Exp Med* **207**:117–128.
Zhou X, Moon C, Zheng F, Luo Y, Soellner D, Nuñez JL, and Wang H (2009) N-methyl-D-aspartate-stimulated ERK1/2 signaling and the transcriptional up-regulation of plasticity-related genes are developmentally regulated following in vitro neuronal maturation. *J Neurosci Res* **87**:2632–2644.

Address correspondence to: Dr. Arianna Bellucci, Division of Pharmacology, Department of Molecular and Translational Medicine, University of Brescia, Viale Europa no. 11, 25123, Brescia, Italy. E-mail: arianna.bellucci@unibs.it

Manuscript Title: **Depletion of progranulin reduces GluN2B-containing NMDA receptor density, tau phosphorylation and dendritic arborization in mouse primary cortical neurons**

Authors: Francesca Longhena, Michela Zaltieri, Jessica Grigoletto, Gaia Faustini, Luca La Via, Roberta Ghidoni, Luisa Benussi, Cristina Missale, PierFranco Spano and Arianna Bellucci

Journal of Pharmacology and Experimental Therapeutics

Supplementary material

Methods

Evaluation of spine density

Cells that were used to analyze spine morphology were transfected at 7 DIV with pCMV-GFP (addgene) by using the LyoVec transfection reagent (InvivoGen, San Diego, CA, USA) according to the manufacturer instructions before to undergo gene silencing. Cells were then analyzed at 72 h from gene silencing. Fluorescence images were collected by using a 63X Plan APO objective (Carl Zeiss, Oberkochen, Germany) and a Zeiss LSM510 confocal microscope (Carl Zeiss, Oberkochen, Germany). Samples were excited by using a 488 nm solid laser and a series of images were acquired in the z dimension at optical slice thickness of 0.5 µm by using the LSM510 Software. Morphometric measurements were analyzed by using ImageJ software (NIH, Bethesda, MD). Analysis were performed in blind for the experimental conditions. For spine density measurements, three dendrite segments or regions of interest (ROI) of fixed length and width were selected per neuron. To avoid potential bias associated with differing spine densities along proximal versus distal dendritic locations, proximal and distal region from a random subset of dendrites were selected. Spine counts were reported as number of spines in 10 µm. Statistical analysis was performed by using one-way ANOVA coupled to Newman-Keuls Multiple Comparison Test.

Antibodies

The following antibodies wer used to recognize GluA1, GluA2 and NR2A subunit: Rabbit polyclonal anti-GluA1 and anti-GluA2 (Alomone labs, Duisburg, Germany) and rabbit polyclonal anti-GluN2A (Merck Millipore, Milano, Italy).

Analysis of the correlation between the number of intersections and the efficiency of PGRN gene silencing in primary cortical neurons exposed to siRNA1, siRNA2, siRNA3 and siRNA4

For analyzing the correlation between the total number of intersections and the efficiency of PGRN gene silencing, the mean ± S.D. of gene silencing efficiency achieved by using the different siRNA sequences was correlated to the mean ± S.D. of the total number of intersections (sum of the intersections detected at 30, 60, 90, 120 and 150 μm from the soma) at 120 h from gene silencing. Data were analyzed by using the Spearman's rank correlation coefficient. 30 photomicrographs for each triplicate sample were analyzed. Experiments were run in triplicate.

Supplementary figure legends

Supplementary figure 1

Influence of PGRN gene silencing on total GluN2A, GluA1 and GluA2 levels and spine density

A. Representative WB images showing absence of GluN2A in primary mouse cortical neurons at 15 DIV. Please note the positive signal in the protein extracts from adult mouse cortex.

B. Western blot analysis showing GluN1 and GluN2B levels in total protein extracts from control, SCR or siRNA exposed cells. Please note the statistically significant decrease of GluN2B levels ($P < 0.001$ Two-way ANOVA + Newman-Keuls Multiple Comparison Test).

C. Western blot analysis showing GluA1 and GluA2 levels in control and SCR or siRNA-exposed primary cortical neurons. Please note that PGRN gene silencing did not significantly affect the levels of GluA2.

D. Analysis of spine density on control, SCR or siRNA-exposed primary cortical neurons at 72 h from gene silencing. Please note the statistically significant reduction of spine density in siRNA exposed neuronal cells when compared to control cells. Scale bar: 5 µm.

Supplementary figure 2

Differential effect of siRNA1, siRNA2, siRNA3 and siRNA4 on neuronal arborization in primary mouse cortical neurons.

A. Representative images showing MAP-2 immunolabeling on siRNA1, siRNA2 siRNA3 and siRNA4-exposed cells. Scale bar: 100 µm.

B. The graph is showing results from the Scholl analysis. Please note that siRNA2 and siRNA3, that were able to induce a reduction of PGRN levels of about 30 % (as shown in Figure 3), only modestly reduced neuronal arborization when compared to siRNA1, that did not lead to PGRN gene silencing in muse primary cortical neurons. Conversely, in the cells exposed to siRNA4, that induced a 60 % decrease of PGRN gene silencing (as shown in figure 3) we detected a significant reduction of neuronal arborizations at 30, 60, 90 and 120 µm from the soma, when compared to those exposed to siRNA1. ° $P < 0.05$ vs siRNA1. *** $P < 0.001$ vs siRNA1.

C. The graph is showing the inverse correlation between the total number of intersections and the efficiency of PGRN gene silencing of siRNA1, siRNA2, siRNA3 and siRNA4 expressed as Spearman rank correlation coefficient.

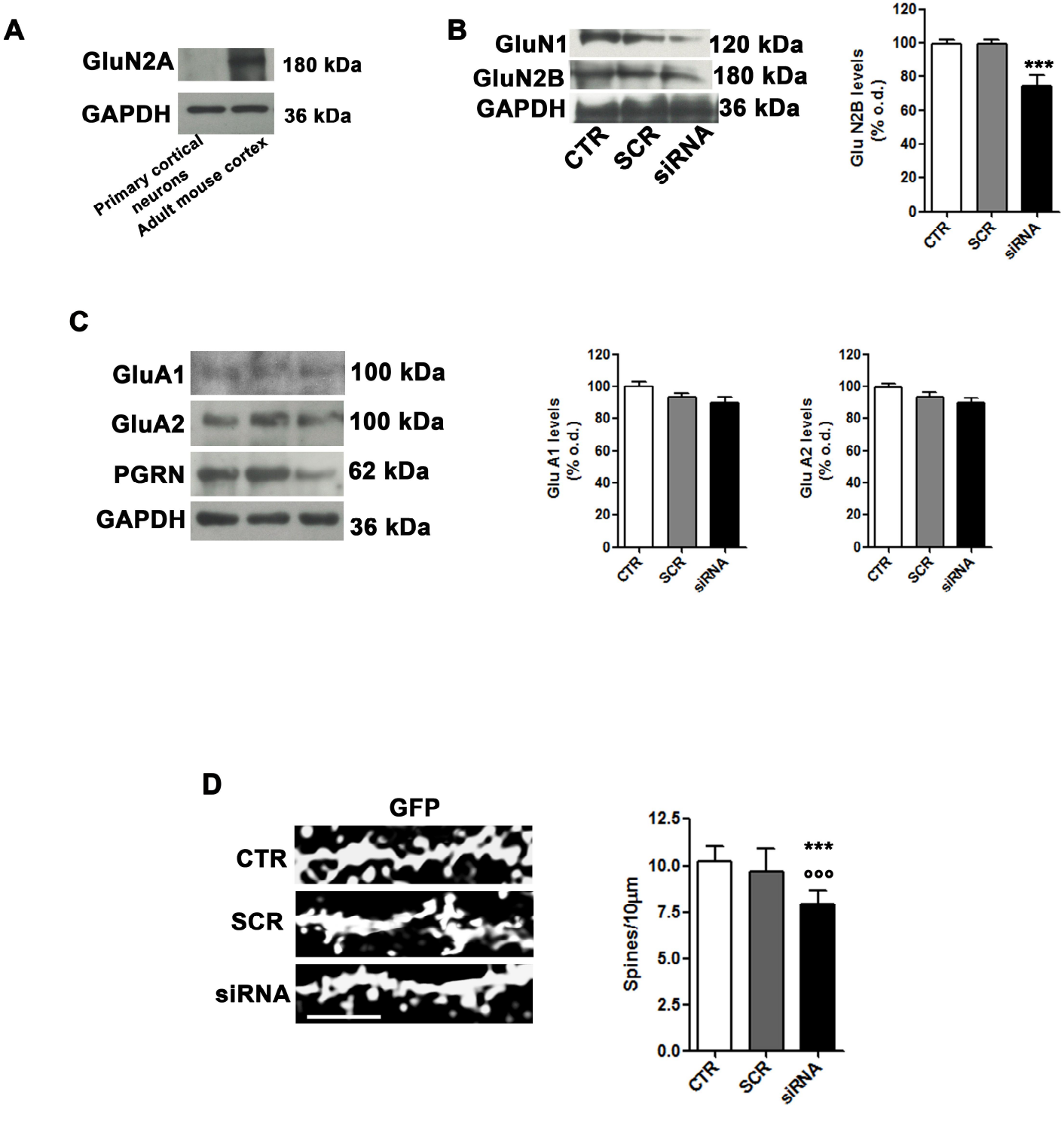

Supplementary figure 1

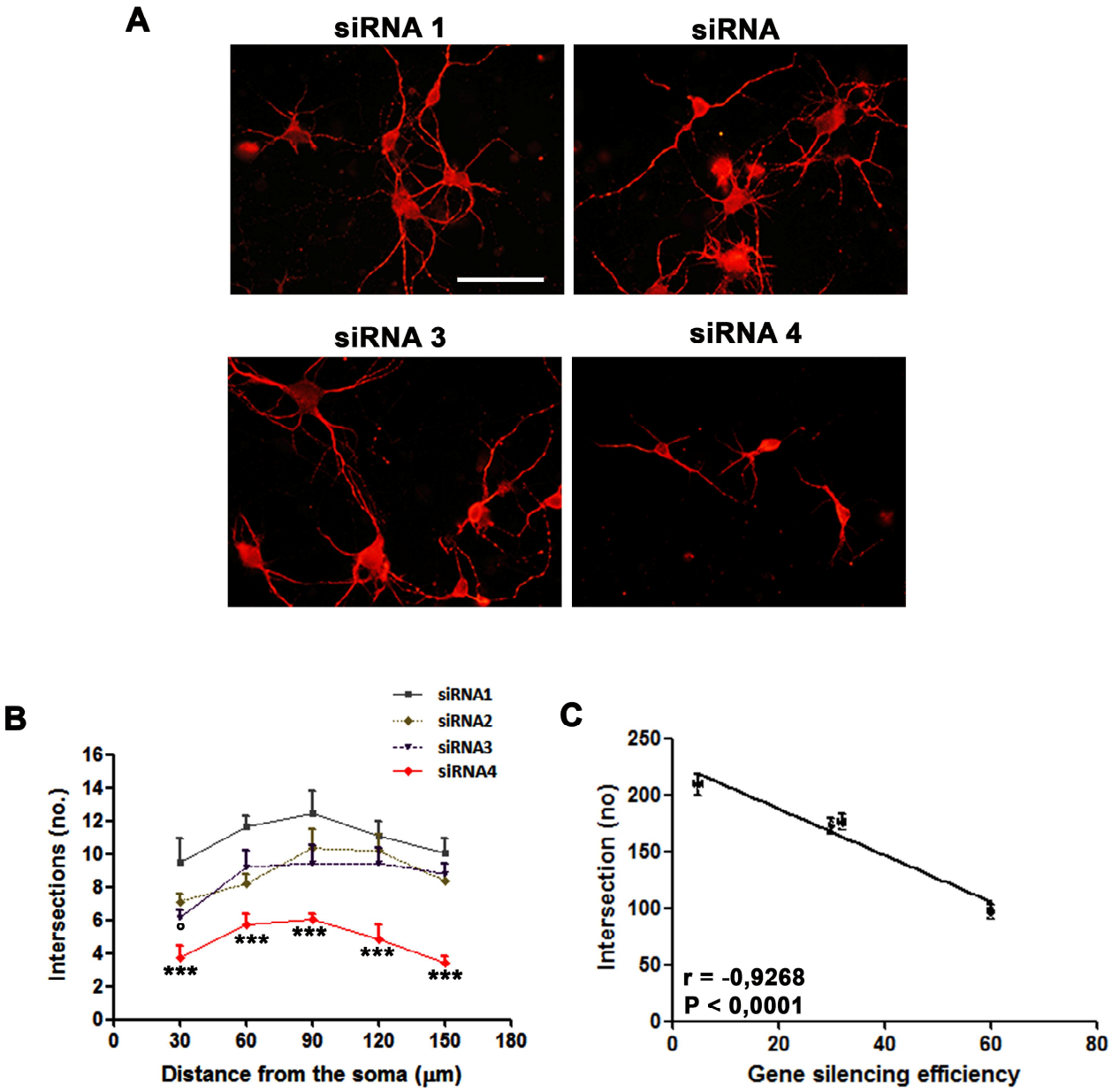

Supplementary figure 2